

Graviton-induced Bremsstrahlung

Erik Dvergsnes^{a,*}, Per Osland^{a,†}, Nurcan Öztürk^{a,b,‡}

^aDepartment of Physics, University of Bergen,
Allégaten 55, N-5007 Bergen, Norway

^bDepartment of Physics, University of Texas,
Arlington, TX 76019, USA

Abstract

We discuss photon Bremsstrahlung induced by virtual graviton exchange in proton-proton interactions at hadronic colliders, resulting from the exchange of Kaluza–Klein excitations of the graviton. The relevant subprocesses, $gg \rightarrow G \rightarrow e^+e^-\gamma$ and $q\bar{q} \rightarrow G \rightarrow e^+e^-\gamma$ are discussed in both the ADD and the RS scenarios. Although two-body final states (or real graviton emission) would presumably be the main discovery channels, a search for three-body final states could be worthwhile since such events have characteristic features that could provide additional confirmation.

*erik.dvergsnes@fi.uib.no

†per.osland@fi.uib.no

‡nurcan@uta.edu

1 Introduction

The idea of additional compact dimensions and strings at the TeV scale, proposed by Antoniadis [1] for solving the hierarchy problem, together with the idea that Standard-model (SM) fields live on branes in a higher-dimensional space [2] have led to the even more radical speculations that extra dimensions might be macroscopic, with SM fields confined to the familiar four-dimensional world (brane) [3, 4]. The models which allow for gravity effects at the TeV scale can be grouped into two kinds, those of factorizable geometry, where the extra dimensions are macroscopic [3] (“ADD scenario”), and those of non-factorizable (warped) geometry, with only one extra dimension separating “our” brane from a hidden brane [4] (“RS scenario”).

In both these scenarios, the propagation of gravitons in the extra dimensions leads to gravitons which from the four-dimensional point of view are massive. In the ADD scenario, these Kaluza–Klein (KK) gravitons have masses starting at values of the order of milli-eV, and there is practically a continuum of them, up to some cut-off M_S (close to the effective Planck scale) of the order of TeV, whereas in the RS scenario they are widely separated resonances with mass splittings of the order of TeV. In both cases, they have a universal coupling to matter and photons via the energy-momentum tensor.

These recent speculations have led to several studies [5–13] of various experimental signals induced by graviton production and exchange. The new scenarios allow for the emission of massive gravitons [5, 6, 7], which would lead to events with missing energy (or transverse momentum), as well as effects due to the exchange of virtual gravitons (in addition to photons and Z s) [5, 7, 8, 11]. These processes include the production of dileptons and diphotons in electron-positron collisions, as well as gluon-gluon and quark-antiquark-induced processes at the Tevatron and LHC.

In fact, several searches at LEP and the Tevatron have given direct bounds on the effective Planck scale, of the order of a TeV [13–15], while astrophysical arguments result in very strong limits when applied to the simplest ADD scenarios, for $n = 2$ and 3 extra dimensions [16]. Of course, the direct experimental searches are most worthwhile. The above studies all focus on two-body final states, which are expected to be dominant, and therefore lead to the most stringent bounds on the existence of extra dimensions.

Here, we shall investigate photon Bremsstrahlung induced by graviton exchange [17]. While this cross section is further reduced by $\mathcal{O}(\alpha/\pi)$, so is the background. It has some characteristic features resulting from the exchange of a spin-2 particle and from the direct graviton-photon coupling, that we would like to point out. These features may be useful in discriminating any signal against the background.

Specifically, we shall consider the process

$$pp \rightarrow e^+e^-\gamma + X, \tag{1.1}$$

which may get a contribution due to graviton exchange, and which for energetic electrons (or muons) and photons should experimentally be a very clean signal. (There is also a related process, where a graviton is emitted in the final state [18].)

Since this final state is very distinct, and since the Standard-model (Drell–Yan) background is well understood, the process (1.1) may offer some hope for observing a signal or improving on the exclusion bounds.

This paper is organized as follows: First (Sec. 2) we consider the gluon-gluon fusion contribution to both two-body and three-body final states. Then (Sec. 3) we consider quark-antiquark annihilation, which also gives rise to the Standard-model background. We calculate the cross section by summing over the KK tower within the ADD (Sec. 4) and RS (Sec. 5) scenarios for a selected choice of parameters, and finally we give some concluding remarks (Sec 6).

2 Gluon-gluon fusion

We shall first discuss gluon-gluon fusion. Due to increasing gluon luminosity at high energies (LHC), this contribution will be dominant for a certain range in invariant mass of the (three-body) final state. At higher invariant masses, the quark-antiquark annihilation may also be important.

2.1 Two-body final states

The process of interest, Eq. (1.1), is related to the two-body final state

$$pp \rightarrow e^+e^- + X \quad (2.1)$$

which may proceed via gluon-gluon fusion and an intermediate graviton,

$$gg \rightarrow G \rightarrow e^+e^-. \quad (2.2)$$

For massless electrons, the cross section for single graviton exchange resulting from gluon-gluon fusion is (in agreement with the results of [12])

$$\hat{\sigma}_{gg \rightarrow ee}^{(G)} = \frac{\kappa^4}{10240\pi} \frac{\hat{s}^3}{(\hat{s} - m_{\vec{n}}^2)^2 + (m_{\vec{n}}\Gamma_{\vec{n}})^2}, \quad (2.3)$$

with $\hat{s} = (k_1 + k_2)^2$ the two-gluon invariant mass squared. Furthermore, $m_{\vec{n}}$ and $\Gamma_{\vec{n}}$ are the mass and width of the graviton¹, and κ is the graviton coupling, to be defined below. The angular distribution, which is forward-backward symmetric, is given by $1 - \cos^4\theta$, where θ is the c.m. scattering angle.

With ξ_1 and ξ_2 the fractional momenta of the two gluons, $k_1 = \xi_1 P_1$, $k_2 = \xi_2 P_2$, and P_1 and P_2 the proton momenta, $(P_1 + P_2)^2 = s$, we have $\hat{s} \simeq \xi_1 \xi_2 s$. For the over-all process (2.1) we thus find the differential cross section

$$\frac{d\sigma_{gg \rightarrow ee}^{(G)}}{d\hat{s}} = \int_0^1 d\xi_1 \int_0^1 d\xi_2 f_g(\xi_1) f_g(\xi_2) \frac{d\hat{\sigma}_{gg \rightarrow ee}^{(G)}}{d\hat{s}}$$

¹The Kaluza–Klein index, \vec{n} on $m_{\vec{n}}$ and $\Gamma_{\vec{n}}$ should not be confused with n , the number of extra dimensions.

$$= \int_0^1 d\xi_1 \int_0^1 d\xi_2 f_g(\xi_1) f_g(\xi_2) \delta(\xi_1 \xi_2 s - \hat{s}) \hat{\sigma}_{gg \rightarrow ee}^{(G)}(\hat{s}) = \frac{1}{s} I_{gg}(\hat{s}) \hat{\sigma}_{gg \rightarrow ee}^{(G)}(\hat{s}), \quad (2.4)$$

with the relevant convolution integral, $I_{gg}(\hat{s})$, over the gluon distribution functions given by Eq. (A.1) in Appendix A.

2.2 Three-body final states

Let us now consider the contribution from gluon-gluon fusion to the Bremsstrahlung process in Eq. (1.1). The underlying subprocess,

$$gg \rightarrow G \rightarrow e^+ e^- \gamma, \quad (2.5)$$

can proceed via the four Feynman diagrams of Fig. 1, the basic couplings for which are given by Han et al. [7] (see also Giudice et al. [5]).

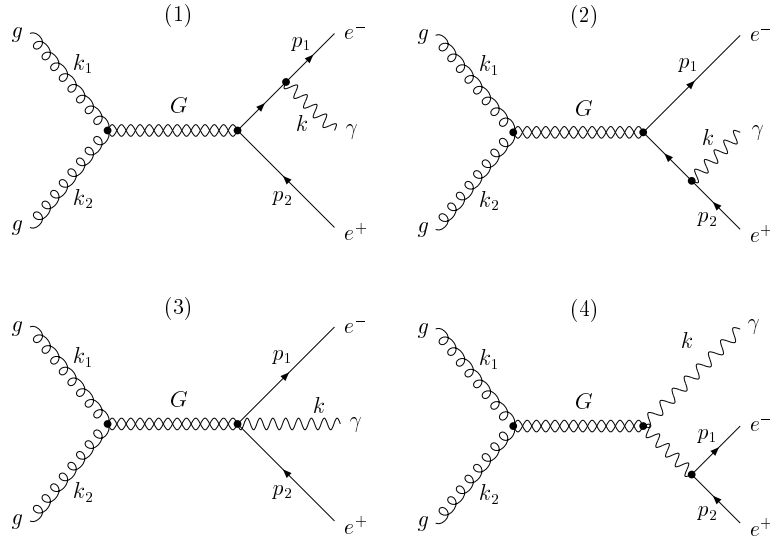


Figure 1: Feynman diagrams for $gg \rightarrow G \rightarrow e^+ e^- \gamma$.

The evaluation of the cross section is straightforward, and the differential cross section (w.r.t. the azimuthal angle, χ , and $\cos \theta$, where θ is the angle between the photon and the beam) is of fourth order in the invariants. This is due to the underlying mechanism being the exchange of a spin-2 object. It is straight-forward to verify that it is gauge invariant with respect to the gluons, as well as to the photon (actually, diagram 4 is by itself gauge invariant). But the expression is quite lengthy, so we shall not write it out here.

The angular distribution of the (two-body) non-radiative cross section (2.3) is given by fourth-order polynomials in $\cos \theta$. Here, just like in gluon Bremsstrahlung (see, e.g., [19]),

there is an accompanying dependence on the azimuthal angle χ , but now up to fourth order in $\cos \chi$, or, equivalently, up to $\cos 4\chi$.

After integrating over the azimuthal orientation of the events, the cross section is of the form

$$\frac{d^2 \hat{\sigma}_{gg \rightarrow ee\gamma}^{(G)}}{dx_1 dx_2} \sim a_0(x_1, x_2) + a_2(x_1, x_2) \cos^2 \theta + a_4(x_1, x_2) \cos^4 \theta, \quad (2.6)$$

similar to the two-body final states, i.e., the gluon-gluon fusion does not contribute to any forward-backward asymmetry.

In our calculations we have chosen the unitary gauge ($\xi^{-1} = 0$ in the notation of [7]), whereby the scalar exchange decouples. After averaging and summing over gluon, electron and photon polarizations, and integrating over event orientations w.r.t. the gluon momentum, we find (for exchange of a single graviton)

$$\frac{d^2 \hat{\sigma}_{gg \rightarrow ee\gamma}^{(G)}}{dx_1 dx_2} = \frac{\alpha \kappa^4 Q_e^2}{2560 \pi^2} \frac{\hat{s}^3}{(\hat{s} - m_{\vec{n}}^2)^2 + (m_{\vec{n}} \Gamma_{\vec{n}})^2} \frac{X_4(x_1, x_2)}{(1 - 2x_1)(1 - 2x_2)(1 - 2x_3)}, \quad (2.7)$$

with $X_4(x_1, x_2)$ given by Eq. (A.3) in Appendix A. Furthermore, α is the fine-structure constant, $Q_e = -1$ is the electron charge, and x_1, x_2 and x_3 denote the fractional energies of the electrons and the photon in the c.m. frame,

$$x_1 = E_1/\sqrt{\hat{s}}, \quad x_2 = E_2/\sqrt{\hat{s}}, \quad x_3 = \omega/\sqrt{\hat{s}}, \quad 0 \leq x_i \leq \frac{1}{2}, \quad (2.8)$$

with $x_1 + x_2 + x_3 = 1$. The denominator in Eq. (2.7) exhibits the familiar singularities in the infrared and collinear limits, $s_1 \equiv (p_1 + k)^2 = \hat{s}(1 - 2x_2) \rightarrow 0$, $s_2 \equiv (p_2 + k)^2 = \hat{s}(1 - 2x_1) \rightarrow 0$, as well as a collinear singularity at $s_3 \equiv (p_1 + p_2)^2 = \hat{s}(1 - 2x_3) \rightarrow 0$ due to the fourth Feynman diagram. Here $\hat{s} \equiv (k_1 + k_2)^2 = (p_1 + p_2 + k)^2$. The additional singularity means that there is a tendency to have events with hard photons [17]. This is one way in which these events differ from ordinary QED-based Bremsstrahlung.

The differential cross section in Eq. (2.7) can be written more compactly as

$$\frac{1}{\hat{\sigma}_{gg \rightarrow ee}^{(G)}} \frac{d^2 \hat{\sigma}_{gg \rightarrow ee\gamma}^{(G)}}{dx_1 dx_2} = \frac{4\alpha Q_e^2}{\pi} \frac{X_4(x_1, x_2)}{(1 - 2x_1)(1 - 2x_2)(1 - 2x_3)}, \quad (2.9)$$

with $\hat{\sigma}_{gg \rightarrow ee}^{(G)}$ given by Eq. (2.3). As we see, the cross section is reduced by a factor $\mathcal{O}(\alpha/\pi)$ compared to the two-body cross section.

Analogous to Eq. (2.4), we find for the gluon contribution to the over-all process (1.1)

$$\frac{d^3 \sigma_{gg \rightarrow ee\gamma}^{(G)}}{d\hat{s} dx_1 dx_2} = \frac{1}{s} I_{gg}(\hat{s}) \frac{d^2 \hat{\sigma}_{gg \rightarrow ee\gamma}^{(G)}}{dx_1 dx_2}, \quad (2.10)$$

with the convolution integral given by Eq. (A.1) in Appendix A.

3 Quark-antiquark annihilation

Another process which contributes to (1.1) is quark-antiquark annihilation. As we shall see, this contribution becomes important for larger invariant masses of the final state.

3.1 Two-body final states

The process in Eq. (2.1) may also proceed via quark-antiquark annihilation and an intermediate graviton, with the following cross section for single graviton exchange (initial state quarks are considered massless)

$$\hat{\sigma}_{q\bar{q} \rightarrow ee}^{(G)} = \frac{\kappa^4}{15360\pi} \frac{\hat{s}^3}{(\hat{s} - m_{\tilde{n}}^2)^2 + m_{\tilde{n}}^2 \Gamma_{\tilde{n}}^2}, \quad (3.1)$$

in agreement with [5, 12]. It differs from the cross section for gluon-gluon fusion by a factor $2/3$.

There is also a SM background to this process, where the same final state is produced through photon or Z exchange. This well-known cross section is given by

$$\hat{\sigma}_{q\bar{q} \rightarrow ee}^{(\text{SM})} = \frac{4\pi\alpha^2}{9\hat{s}} [Q_q^2 Q_e^2 + 2Q_q Q_e v_q v_e \text{Re} \chi(\hat{s}) + (v_q^2 + a_q^2)(v_e^2 + a_e^2) |\chi(\hat{s})|^2], \quad (3.2)$$

with

$$\chi(\hat{s}) = \frac{1}{\sin^2(2\theta_W)} \frac{\hat{s}}{(\hat{s} - m_Z^2) + im_Z \Gamma_Z}, \quad (3.3)$$

where we have normalized vector and axial-vector couplings to $v_f = T_f - 2Q_f \sin^2 \theta_W$ and $a_f = T_f$ respectively, with T_f the isospin. Furthermore, m_Z and Γ_Z are the mass and width of the Z boson, Q_q the quark charge, and θ_W the weak mixing angle.

In the case of $q\bar{q} \rightarrow G \rightarrow e^+e^-$, with the cross section given by Eq. (3.1), the angular distribution is $1 - 3\cos^2\theta + 4\cos^4\theta$, whereas for the photon exchange, Eq. (3.2), the angular distribution is given by the familiar $1 + \cos^2\theta$. The interference between graviton and photon exchange has an angular distribution given by $\cos^3\theta$ (as pointed out by Ref. [5]) i.e., *it exhibits a forward-backward asymmetry* and vanishes upon integration. The interference between graviton and Z exchange exhibits a slightly different angular distribution (which also vanishes upon integration).

For pp collisions, we find the graviton contribution to the differential cross section (in accordance with Eq. (2.4))

$$\frac{d\sigma_{q\bar{q} \rightarrow ee}^{(G)}}{d\hat{s}} = \frac{1}{s} I_{q\bar{q}}(\hat{s}) \hat{\sigma}_{q\bar{q} \rightarrow ee}^{(G)}(\hat{s}), \quad (3.4)$$

with $I_{q\bar{q}}(\hat{s})$ given in Appendix A. The SM contribution can be found in a similar manner, but here the convolution integrals must be weighted by the factors Q_q^2 , $Q_q v_q$ and $(v_q^2 + a_q^2)$ for photon exchange, interference between the photon and the Z , and for Z exchange, respectively (see Appendix A). The reason for this is that the convolution integral implicitly contains flavor summation.

3.2 Three-body final states

Now we will examine the subprocess

$$q\bar{q} \rightarrow \gamma, Z, G \rightarrow e^+e^-\gamma \quad (3.5)$$

which is determined by the diagrams of Fig. 2, together with the SM background, which arises from diagrams similar to diagrams 1 and 2 with a γ or Z exchanged instead of the graviton. We shall refer to these contributions as

$$\hat{\sigma}_{q\bar{q} \rightarrow ee\gamma}^{(\text{SM})}, \quad \hat{\sigma}_{q\bar{q} \rightarrow ee\gamma}^{(G)}, \quad \hat{\sigma}_{q\bar{q} \rightarrow ee\gamma}^{(G,\gamma)}, \quad \text{and} \quad \hat{\sigma}_{q\bar{q} \rightarrow ee\gamma}^{(G,Z)}, \quad (3.6)$$

where the first term is the Standard-model background, the second term is the graviton contribution and the last two are graviton-photon and graviton- Z interference terms, respectively. Compared to gluon-gluon fusion, there is the additional diagram 5 involving graviton exchange, due to the $G\gamma\gamma$ coupling.

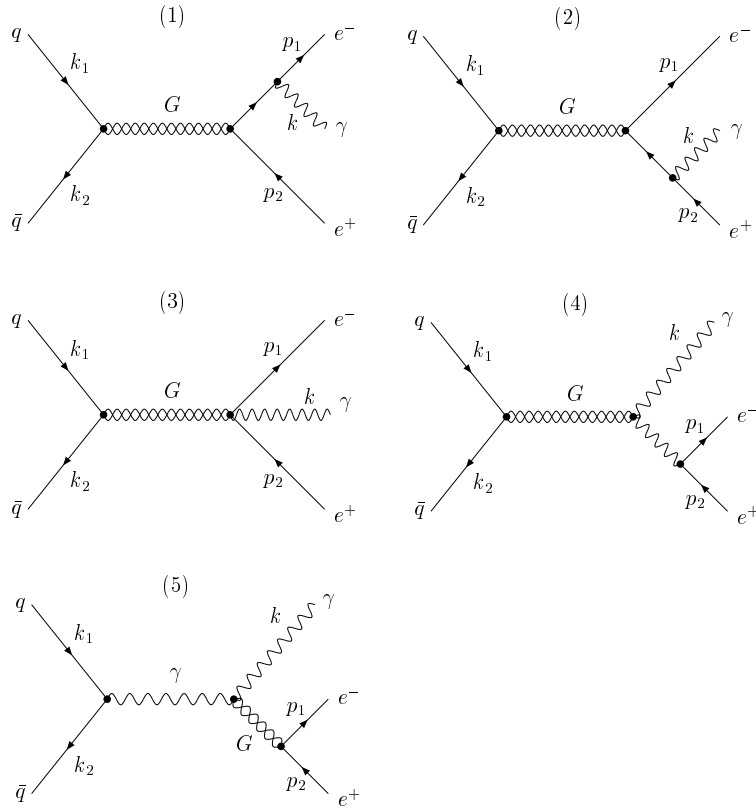


Figure 2: Feynman diagrams for $q\bar{q} \rightarrow G \rightarrow e^+e^-\gamma$.

First we shall consider the graviton exchange diagrams of Fig. 2, where we introduce the following notation,

$$\hat{\sigma}_{q\bar{q} \rightarrow ee\gamma}^{(G)} = \hat{\sigma}_4^{(G)} + \hat{\sigma}_5^{(G)} + \hat{\sigma}_{4,5}^{(G)}. \quad (3.7)$$

It is convenient to separate diagram 5 from the other diagrams since, in this case, the graviton propagator does not carry all the momentum of the initial quarks.

For the first four diagrams, we find

$$\frac{d^2 \hat{\sigma}_4^{(G)}}{dx_1 dx_2} = \frac{\alpha \kappa^4 Q_e^2}{3840 \pi^2} \frac{\hat{s}^3}{(\hat{s} - m_{\tilde{n}}^2)^2 + (m_{\tilde{n}} \Gamma_{\tilde{n}})^2} \frac{X_4(x_1, x_2)}{(1 - 2x_1)(1 - 2x_2)(1 - 2x_3)}, \quad (3.8)$$

with $X_4(x_1, x_2)$ given by Eq. (A.3). This contribution is, as in the two-body case, identical to the contribution from gluon-gluon fusion, except for a factor of 2/3.

The fifth diagram gives a somewhat different contribution,

$$\frac{d^2 \hat{\sigma}_5^{(G)}}{dx_1 dx_2} = \frac{\alpha \kappa^4 Q_q^2}{1152 \pi^2} \frac{\hat{s}^3}{(s_3 - m_{\tilde{n}}^2)^2 + (m_{\tilde{n}} \Gamma_{\tilde{n}})^2} X_5(x_1, x_2), \quad (3.9)$$

where $X_5(x_1, x_2)$ is given by Eq. (A.3) in Appendix A. Since the denominator in Eq. (3.9) depends on $s_3 = (1 - 2x_3)\hat{s}$ instead of \hat{s} , this contribution will be smeared out when integrated over x_3 , therefore it does not contribute to any sharp resonance in neither of the two scenarios.

There is also an interference term, $\hat{\sigma}_{4,5}^{(G)}$, between diagrams 1–4 and 5, which has to be considered. It contributes to the forward-backward asymmetry, and vanishes when integrated over all event orientations.

In the three-body case, the SM background becomes²

$$\frac{d^2 \hat{\sigma}_{q\bar{q} \rightarrow ee\gamma}^{(\text{SM})}}{dx_1 dx_2} = \frac{4\alpha Q_e^2}{\pi} \hat{\sigma}_{q\bar{q} \rightarrow ee}^{(\text{SM})} \frac{X_{\text{SM}}(x_1, x_2)}{(1 - 2x_1)(1 - 2x_2)} \quad (3.10)$$

with $X_{\text{SM}}(x_1, x_2)$ given in Appendix A, and $\hat{\sigma}_{q\bar{q} \rightarrow ee}^{(\text{SM})}$ given by Eq. (3.2). This is the familiar Bremsstrahlung cross section expressed in terms of the related two-body process.

We shall now introduce the following notation for the interference terms between graviton exchange and the SM diagrams:

$$\begin{aligned} \hat{\sigma}_{q\bar{q} \rightarrow ee\gamma}^{(G,\gamma)} &= \hat{\sigma}_4^{(G,\gamma)} + \hat{\sigma}_5^{(G,\gamma)}, \\ \hat{\sigma}_{q\bar{q} \rightarrow ee\gamma}^{(G,Z)} &= \hat{\sigma}_4^{(G,Z)} + \hat{\sigma}_5^{(G,Z)}, \end{aligned} \quad (3.11)$$

where the first terms are interferences of the first four diagrams in Fig. 2 with the SM background, and the last terms are interferences of the fifth diagram with the SM background.

We find that both γ and Z interferences with diagrams 1–4 vanish after integration over event orientations, but they contribute to the forward-backward asymmetry. For the non-vanishing terms (interference between diagram 5 and the SM background), we get

$$\frac{d^2 \hat{\sigma}_5^{(G,\gamma)}}{dx_1 dx_2} = -\frac{\alpha^2 \kappa^2 Q_q^2 Q_e^2 \hat{s}}{9\pi} \text{Re} \left[\frac{1}{s_3 - m_{\tilde{n}}^2 + im_{\tilde{n}} \Gamma_{\tilde{n}}} \right] X_{5,\gamma}(x_1, x_2),$$

²Radiation off initial quarks has been neglected here. It can be substantially reduced by suitable cuts.

$$\frac{d^2 \hat{\sigma}_5^{(G,Z)}}{dx_1 dx_2} = -\frac{\alpha^2 \kappa^2 Q_q Q_e v_q v_e \hat{s}}{9\pi} \text{Re} \left[\chi^*(\hat{s}) \frac{1}{s_3 - m_{\vec{n}}^2 + i m_{\vec{n}} \Gamma_{\vec{n}}} \right] X_{5,Z}(x_1, x_2), \quad (3.12)$$

where $\chi(\hat{s})$ is given by Eq. (3.3), and $X_{5,\gamma}(x_1, x_2) = X_{5,Z}(x_1, x_2)$ given in Appendix A.

To find the contribution from quark-antiquark annihilation to the over-all process (1.1), a relation similar to the one given by Eq. (3.4) should be used. However, in the case of the SM background and its interference with diagram 5, when there are quark charges and vector/axial-vector couplings involved, the convolution integrals must be weighted by these factors, as shown in Appendix A.

4 Bremsstrahlung in the ADD scenario

In the ADD scenario [3], the coupling of each KK mode to matter is Planck-scale suppressed. However, since the states are very closely spaced, with [7]

$$m_{\vec{n}}^2 = \frac{4\pi^2 \vec{n}^2}{R^2}, \quad (4.1)$$

and $R/2\pi$ the compactification radii, the coherent summation over the many modes leads to effective couplings with strength $1/M_S$, where M_S is the UV cut-off (close to the effective Planck scale).

Explicitly, in this scenario, the graviton coupling is in the $(4+n)$ -dimensional theory given by [7]

$$\hat{g}_{MN} = \hat{\eta}_{MN} + \hat{\kappa} \hat{h}_{MN}, \quad \hat{\kappa}^2 = 16\pi G_N^{(4+n)}, \quad (4.2)$$

where $G_N^{(4+n)}$ is Newton's constant in $4+n$ dimensions. In 4 dimensions the coupling can be written as

$$\kappa^2 = V_n^{-1} \hat{\kappa}^2 = 16\pi V_n^{-1} G_N^{(4+n)} = 16\pi G_N, \quad (4.3)$$

with V_n the volume of the n -dimensional compactified space ($V_n = R^n$ for a torus T^n) and G_N the 4-dimensional Newton constant.

Summing coherently over all KK modes in a tower, the graviton propagator gets replaced [7]:

$$\frac{1}{\hat{s} - m_{\vec{n}}^2 + i m_{\vec{n}} \Gamma_{\vec{n}}} \equiv -iD(\hat{s}) \rightarrow \frac{\hat{s}^{n/2-1}}{\Gamma(n/2)} \frac{R^n}{(4\pi)^{n/2}} [2I(M_S/\sqrt{\hat{s}}) - i\pi], \quad (4.4)$$

with

$$I(M_S/\sqrt{\hat{s}}) = \begin{cases} -\sum_{k=1}^{n/2-1} \frac{1}{2k} \left(\frac{M_S}{\sqrt{\hat{s}}} \right)^{2k} - \frac{1}{2} \log \left(\frac{M_S^2}{\hat{s}} - 1 \right), & n = \text{even}, \\ -\sum_{k=1}^{(n-1)/2} \frac{1}{2k-1} \left(\frac{M_S}{\sqrt{\hat{s}}} \right)^{2k-1} + \frac{1}{2} \log \left(\frac{M_S + \sqrt{\hat{s}}}{M_S - \sqrt{\hat{s}}} \right), & n = \text{odd}. \end{cases} \quad (4.5)$$

for n extra dimensions.

Higher order loop effects may be important [20], so these expressions should not be taken too literally. In particular, this applies to the dependence on the number of extra dimensions. In the approach of [5] and [8] this uncertainty, including the n -dependence, is absorbed in the cut-off so that $D(\hat{s})$ and $D(s_3)$ (see Fig. 2 and Eq. (4.4)) are indistinguishable. Here, in order to preserve the qualitative difference between these two propagators, we shall use the expressions of Eq. (4.5).

Invoking the relation [7]

$$\kappa^2 R^n = 8\pi(4\pi)^{n/2}\Gamma(n/2)M_S^{-(n+2)} \quad (4.6)$$

between the volume of the extra dimensions, the gravitational coupling and the cut-off scale, the differential cross section can be expressed as

$$\begin{aligned} \frac{d^3\sigma}{d\hat{s}dx_1dx_2} = & \frac{\alpha}{40sM_S^2} \left\{ Q_e^2 \left(\frac{\hat{s}}{M_S^2} \right)^{n+1} [I_{gg}(\hat{s}) + \frac{2}{3}I_{q\bar{q}}(\hat{s})] \right. \\ & \times \left[4I^2(M_S/\sqrt{\hat{s}}) + \pi^2 \right] \frac{X_4(x_1, x_2)}{(1-2x_1)(1-2x_2)(1-2x_3)} \\ & + \frac{20}{9} \frac{s_3^{n-2}\hat{s}^3}{M_S^{2n+2}} I_{q\bar{q}}^{(\gamma)}(\hat{s}) [4I^2(M_S/\sqrt{s_3}) + \pi^2] X_5(x_1, x_2) \\ & - \frac{320\alpha}{9} \frac{s_3^{n/2-1}\hat{s}}{M_S^n} \left[2Q_e^2 I_{q\bar{q}}^{(\gamma)}(\hat{s}) I(M_S/\sqrt{s_3}) X_{5,\gamma}(x_1, x_2) \right. \\ & \left. \left. + Q_e v_e I_{q\bar{q}}^{(\gamma,Z)}(\hat{s}) \operatorname{Re} \{ \chi^*(\hat{s}) [2I(M_S/\sqrt{s_3}) - i\pi] \} X_{5,Z}(x_1, x_2) \right] \right\} \\ & + \frac{16\alpha^3 Q_e^2}{9s\hat{s}} [Q_e^2 I_{q\bar{q}}^{(\gamma)}(\hat{s}) + 2Q_e v_e I_{q\bar{q}}^{(\gamma,Z)}(\hat{s}) \operatorname{Re} \chi(\hat{s}) \\ & + (v_e^2 + a_e^2) I_{q\bar{q}}^{(Z)}(\hat{s}) |\chi(\hat{s})|^2] \frac{X_{\text{SM}}(x_1, x_2)}{(1-2x_1)(1-2x_2)}, \end{aligned} \quad (4.7)$$

where $\chi(\hat{s})$ is given by Eq. (3.3) and the convolution integrals are given in Appendix A. In this Eq. (4.7), the different contributions are given in the following order: First gluon-gluon fusion and quark-antiquark annihilation (diagrams 1–4), then quark-antiquark annihilation (diagram 5), interference between the fifth diagram and photon exchange, interference between the fifth diagram and Z exchange, and finally the SM background. The origins of the different terms are reflected in the subscripts of the X 's.

In Fig. 3, we show the cross section, differential w.r.t. $\sqrt{\hat{s}}$ (labeled $M_{e\bar{e}\gamma}$ in the figures), for $M_S = 4$ TeV and $n = 2, 3, 4, 5$ and 6 (left panel) in the ADD scenario, where we have integrated out the x_1, x_2 dependence (see Appendix B). The right panel shows only the $n = 2$ curve, with the contributions from gluon-gluon fusion and quark-antiquark annihilation (induced by graviton exchange) also displayed. Note that gluon-gluon fusion is dominant from $\sqrt{\hat{s}} \simeq 1$ TeV up to $\sqrt{\hat{s}} \simeq 3$ TeV for this choice of parameters, whereas the quark-antiquark annihilation process takes over at larger invariant masses.

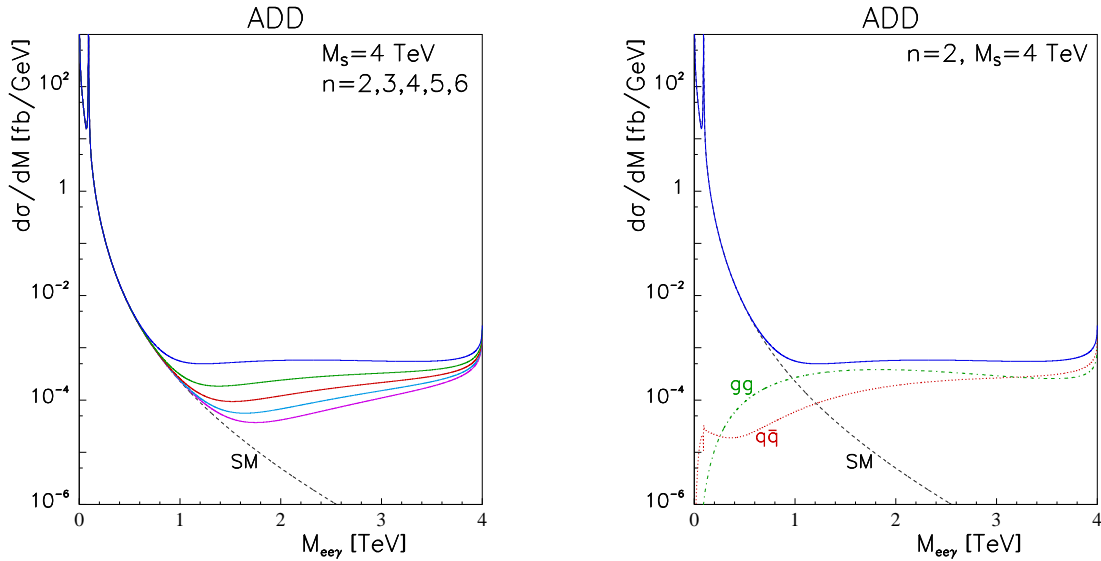


Figure 3: Cross sections for $pp \rightarrow e^+e^-\gamma$ at $\sqrt{s} = 14$ TeV. Both plots are for the ADD model with $M_S = 4$ TeV. We have set the number of extra dimensions (from above) to $n = 2, 3, 4, 5$, and 6 for the left panel. The full differential cross section, $d\sigma/d\sqrt{\hat{s}}$ (solid), and the SM background (dashed) are shown in both plots, whereas the gg (dash-dotted) and the $q\bar{q}$ contributions (dotted) are shown in the right panel for $n = 2$.

We have integrated over $x_3^{\min} \leq x_3 \leq 0.5$, subject to the y -cuts: $s_1, s_2 \geq y\hat{s}$, $s_3 \geq y_3\hat{s}$, where both $y = y_3 = 0.01$. The minimum invariant mass of the two electrons is controlled by y_3 . At a scale $\sqrt{\hat{s}} = 1$ TeV, the cut of $y = 0.01$ corresponds to electron (or photon) energies exceeding 10 GeV. We consider a minimum x_3 of 0.1 in these plots. The corresponding angular cuts are well within the resolutions foreseen at the LHC [21].

Here, we have taken $\sqrt{s} = 14$ TeV, which corresponds to the LHC energy. With an integrated luminosity of 100 fb^{-1} and a bin-width of 100 GeV, we might expect a few events per bin at invariant masses above 1 TeV.

Close to the cut-off, M_S , the cross section blows up due to the logarithm in $I(M_S/\sqrt{\hat{s}})$. This is of course an artifact, due to the way the cut-off is treated [20]. Note that the explicit n -dependence in Fig. 3 is in the approach of [5, 8] absorbed in the cut-off.

Naively, one might have expected the interference between the SM background and the graviton-mediated amplitudes (the bump in the $q\bar{q}$ curve) to be important. This is not the case. First of all, the SM amplitude only interferes with the $q\bar{q}$ -annihilation part of the graviton-mediated amplitude. Secondly, the interference with the largest part of the $q\bar{q}$ annihilation amplitude, given by diagrams 1–4 of Fig. 2, only contributes to asymmetries which anyway vanish at the LHC.

The part of the $q\bar{q}$ annihilation amplitude which is given by diagram 5 is everywhere significantly smaller than the gg amplitude (by more than two orders of magnitude). This is mainly due to the difference in the integrals over x_1, x_2 , which in the case of gg con-

tains $X_4(x_1, x_2)$ together with three singularities, whereas for diagram 5 it only contains $X_5(x_1, x_2)$ (and factors involving s_3). At lower values of invariant mass, the convolution integrals also favor the gg term.

Therefore, in order for the interference between the SM amplitude and diagram 5 of the $q\bar{q}$ -annihilation amplitude to be comparable to the gg contribution, the SM amplitude needs to be much larger than the signal. This is true only for low values of invariant mass, but here the SM background will dominate completely, and therefore the interference terms are nowhere important.

5 Bremsstrahlung in the RS scenario

In the Randall–Sundrum scenario [4], the graviton masses are given by [10]

$$m_n = kx_n e^{-kr_c\pi} = \frac{x_n}{x_1} m_1, \quad (5.1)$$

where x_n are roots of the Bessel function³ of order 1, $J_1(x_n) = 0$, k is of the order of the (four-dimensional) Planck scale and r_c the compactification radius of the extra dimension⁴. Since there is only one extra dimension in this scenario, we shall use m_n instead of $m_{\tilde{n}}$ for the mass of the n th graviton.

The gravitational coupling is in this model given by [10, 12]

$$\kappa = \sqrt{16\pi} \frac{x_n}{m_n} \frac{k}{M_{\text{Pl}}} = \sqrt{2} \frac{x_1}{m_1} \frac{k}{\overline{M}_{\text{Pl}}}, \quad \overline{M}_{\text{Pl}} = \frac{M_{\text{Pl}}}{\sqrt{8\pi}} = 2.4 \times 10^{18} \text{ GeV}. \quad (5.2)$$

Here we shall use m_1 and $k/\overline{M}_{\text{Pl}}$ as the two parameters which specify the model. Note that $0.01 \leq k/\overline{M}_{\text{Pl}} \leq 1$ [10].

The differential cross section can in the RS scenario be expressed as (with the different contributions given in the same order as in Eq. (4.7)):

$$\begin{aligned} \frac{d^3\sigma}{d\hat{s} dx_1 dx_2} = & \frac{\alpha x_1^4 \hat{s}^3}{640\pi^2 m_1^4 s} \left(\frac{k}{\overline{M}_{\text{Pl}}} \right)^4 \\ & \times \left[Q_e^2 [I_{gg}(\hat{s}) + \frac{2}{3} I_{q\bar{q}}(\hat{s})] \left| \sum_n \frac{1}{\hat{s} - m_n^2 + im_n \Gamma_n} \right|^2 \frac{X_4(x_1, x_2)}{(1-2x_1)(1-2x_2)(1-2x_3)} \right. \\ & + \frac{20}{9} I_{q\bar{q}}^{(\gamma)}(\hat{s}) \left| \sum_n \frac{1}{s_3 - m_n^2 + im_n \Gamma_n} \right|^2 X_5(x_1, x_2) \left. \right] \\ & - \frac{2\alpha^2 x_1^2 \hat{s}}{9\pi m_1^2 s} \left(\frac{k}{\overline{M}_{\text{Pl}}} \right)^2 \left[Q_e^2 I_{q\bar{q}}^{(\gamma)}(\hat{s}) \text{Re} \left(\sum_n \frac{1}{s_3 - m_n^2 + im_n \Gamma_n} \right) X_{5,\gamma}(x_1, x_2) \right] \end{aligned}$$

³The first four roots are 3.83, 7.02, 10.17 and 13.32.

⁴To solve the hierarchy problem, $kr_c \sim 12$ is required.

$$\begin{aligned}
& + Q_e v_e I_{q\bar{q}}^{(\gamma, Z)}(\hat{s}) \operatorname{Re} \left(\chi^*(\hat{s}) \sum_n \frac{1}{s_3 - m_n^2 + i m_n \Gamma_n} \right) X_{5, Z}(x_1, x_2) \Big] \\
& + \frac{16\alpha^3 Q_e^2}{9s\hat{s}} \left[Q_e^2 I_{q\bar{q}}^{(\gamma)}(\hat{s}) + 2Q_e v_e I_{q\bar{q}}^{(\gamma, Z)}(\hat{s}) \operatorname{Re} \chi(\hat{s}) \right. \\
& \left. + (v_e^2 + a_e^2) I_{q\bar{q}}^{(Z)}(\hat{s}) |\chi(\hat{s})|^2 \right] \frac{X_{\text{SM}}(x_1, x_2)}{(1 - 2x_1)(1 - 2x_2)}, \tag{5.3}
\end{aligned}$$

where [7, 22]

$$\Gamma_n \equiv \frac{\gamma_G}{20\pi} m_n^3 \kappa^2 = \frac{\gamma_G}{10\pi} x_n^2 m_n \left(\frac{k}{\overline{M}_{\text{Pl}}} \right)^2, \tag{5.4}$$

with

$$\gamma_G = 1 + \chi_\gamma + \chi_Z + \chi_W + \chi_\ell + \chi_q + \chi_H + \chi_r \tag{5.5}$$

the total graviton width in units of the two-gluon width. Neglecting mass effects, we have [7, 22]

$$\begin{aligned}
\chi_\gamma &= \frac{1}{8}, & \chi_Z &= \frac{13}{96}, & \chi_W &= \frac{13}{48}, \\
\chi_\ell &= \frac{N_\ell}{16}, & \chi_q &= \frac{N_c N_q}{16}, & \chi_H &= \chi_r = \frac{1}{48}.
\end{aligned} \tag{5.6}$$

Here, $N_\ell = 6$ is the number of leptons, and $N_c N_q = 18$ is the number of quarks weighted with color factors. Note that since we have neglected quark and electron masses, there is no contribution to the cross section from radion exchange, since the radion couples to the trace of the energy-momentum tensor. However, it contributes slightly to Γ_n through Eq. (5.4).

We display the RS scenario cross section, differential w.r.t. $\sqrt{\hat{s}}$ (see Eq. (5.3)), in Fig. 4. In the left panel, we have summed over KK states, and chosen the first graviton resonance at $m_1 = 1$ TeV, with $k/\overline{M}_{\text{Pl}}$ set to 0.1, 0.05 and 0.01 (from above). In the right panel, we show the different contributions (gg and $q\bar{q}$) to the cross section (for $k/\overline{M}_{\text{Pl}} = 0.05$) induced by graviton exchange. The y -cuts are the same as in the ADD case.

Also in the RS scenario the interference terms are negligible, and the reasons are essentially the same as in the ADD scenario. As we mentioned above, the s_3 dependence will smear out the contribution from diagram 5. For invariant masses greater than

$$\sqrt{\hat{s}} = \frac{m_1}{1 - 2x_3^{\min}}, \tag{5.7}$$

s_3^{\max} will always be greater than m_1 , which means that the first resonance will be integrated over. Since for the interference terms, the cross section is only linear in the propagator pole singularities, we expect diagram 5 to be of greater importance. Beyond the second peak (in the case of $k/\overline{M}_{\text{Pl}} = 0.05$ and $m_1 = 1$ TeV), the contribution from diagram 5 rises above the SM background, but the interferences stay well below.

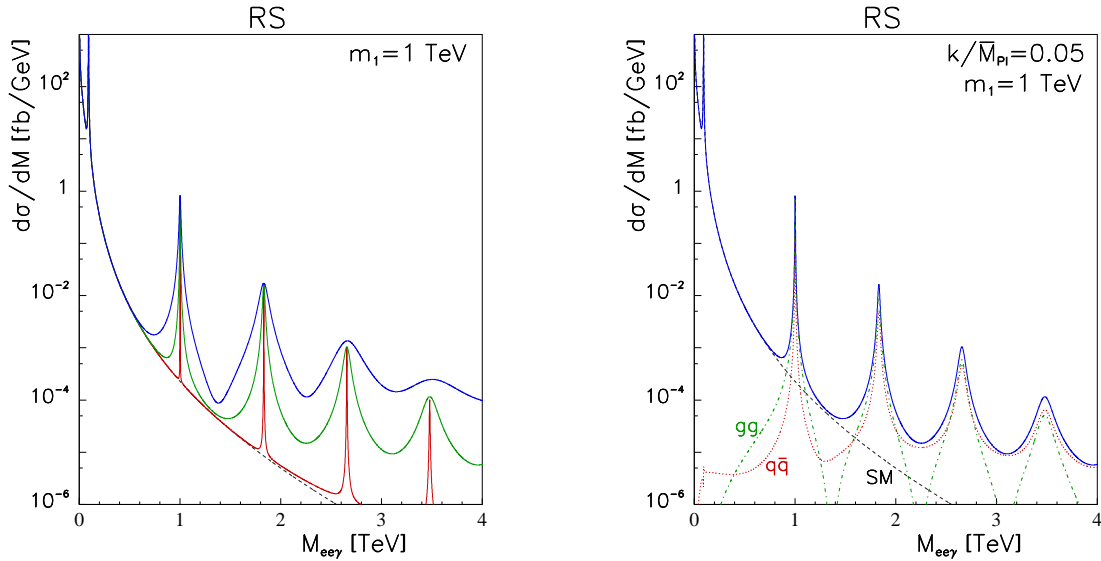


Figure 4: Differential cross sections for the RS model, with $m_1 = 1$ TeV. The left panel shows the differential cross section, $d\sigma/d\sqrt{\hat{s}}$ (solid) with (from above) $k/\overline{M}_{\text{Pl}} = 0.1$, 0.05 and 0.01, and the SM background (dashed). Right panel: the gg (dash dotted) and $q\bar{q}$ (dotted) contributions to the cross section are shown for $k/\overline{M}_{\text{Pl}} = 0.05$.

It should be noted that the third and fourth peaks should be somewhat reduced since we have not taken into account that these gravitons can decay into the first KK resonance. Self-interactions of the gravitons were considered in [23], where a BR of about 15% was found for the $G_3 \rightarrow G_1 G_1$ decay.

By comparing Figs. 3 and 4, we see that the difference between the two scenarios is striking, with extremely narrow, and widely separated resonances in the RS case, compared to the continuum in the ADD case. Note that according to our expressions, the $k/\overline{M}_{\text{Pl}}$ dependence cancels at the resonance. A single peak should therefore have a height which is independent of $k/\overline{M}_{\text{Pl}}$, but at very high invariant masses we see that the $k/\overline{M}_{\text{Pl}} = 0.1$ peak is higher than the other peaks, and also slightly shifted. This is mainly due to interference with, and overlap of the neighboring peaks which are very broad.

Since the cross sections for graviton-induced Bremsstrahlung are much lower than for the corresponding two-body final state, an important question is, however, if there is any chance of seeing these resonances in the experiments. To give an order of magnitude estimate of the number of events to expect from these narrow peaks, we have integrated the differential cross sections given in Fig. 4 over bins in $M_{ee\gamma}$. In the upper left panel of Fig. 5 we integrate over $\sqrt{\hat{s}}$, starting from $\sqrt{\hat{s}} = M_{ee\gamma}^{\text{min}}$. The different curves correspond to $k/\overline{M}_{\text{Pl}} = 0.1$, 0.05 and 0.01 (from above) for $m_1 = 0.5$ (solid), 1 (dotted) and 1.5 TeV (dash-dotted). This should be compared to the SM background (dashed) which is also shown. In the remaining panels of Fig. 5 we have integrated over 100 GeV bins for the same choice of $k/\overline{M}_{\text{Pl}}$, for $m_1 = 0.5$, 1.0 and 1.5 TeV.

We see that for these parameters it should be possible to resolve at least the first peak, and in most cases several peaks are visible. We emphasize that this is not a simulation, but these plots should provide a feeling for the number of events corresponding to these narrow peaks.

6 Concluding remarks

In summary, we have discussed photon Bremsstrahlung induced by the exchange of massive gravitons at hadron colliders, in particular at the LHC. Both the ADD and the RS scenarios have been considered. We found that three-body final states are likely to be detectable, and could be a valuable supplement to the two-body final states, for the purpose of detecting the effects from massive gravitons related to extra dimensions (if such exist). These configurations, of a hard photon associated with an electron–positron (or muon) pair in the opposite direction, should provide a striking signature at the LHC.

We have here focused on Bremsstrahlung at the LHC. At the Fermilab, the phenomenology will be rather different. Because of the lower energy, and because of the different initial state, quark–antiquark annihilation will be much more important, relative to the glue–glue initial state. Furthermore, there will in $p\bar{p}$ collisions be forward–backward asymmetries induced by the interference between the C-odd exchange of a photon or a Z , and the C-even exchange of a graviton. This effect, which is washed out at the LHC because of the C-even initial state, is of course present also for $e^+e^- \rightarrow f\bar{f}$ [8], and will have an analogue in the three-body final states. We hope to discuss this effect elsewhere.

Acknowledgments. It is a pleasure to thank Hans Bijmans, John Ellis, Gian Giudice, JoAnne Hewett, and, in particular, Paolo di Vecchia for very useful discussions. This research has been supported by the Research Council of Norway and by NORDITA. The work of N.Ö. was supported in part by the Robert A. Welch Foundation.

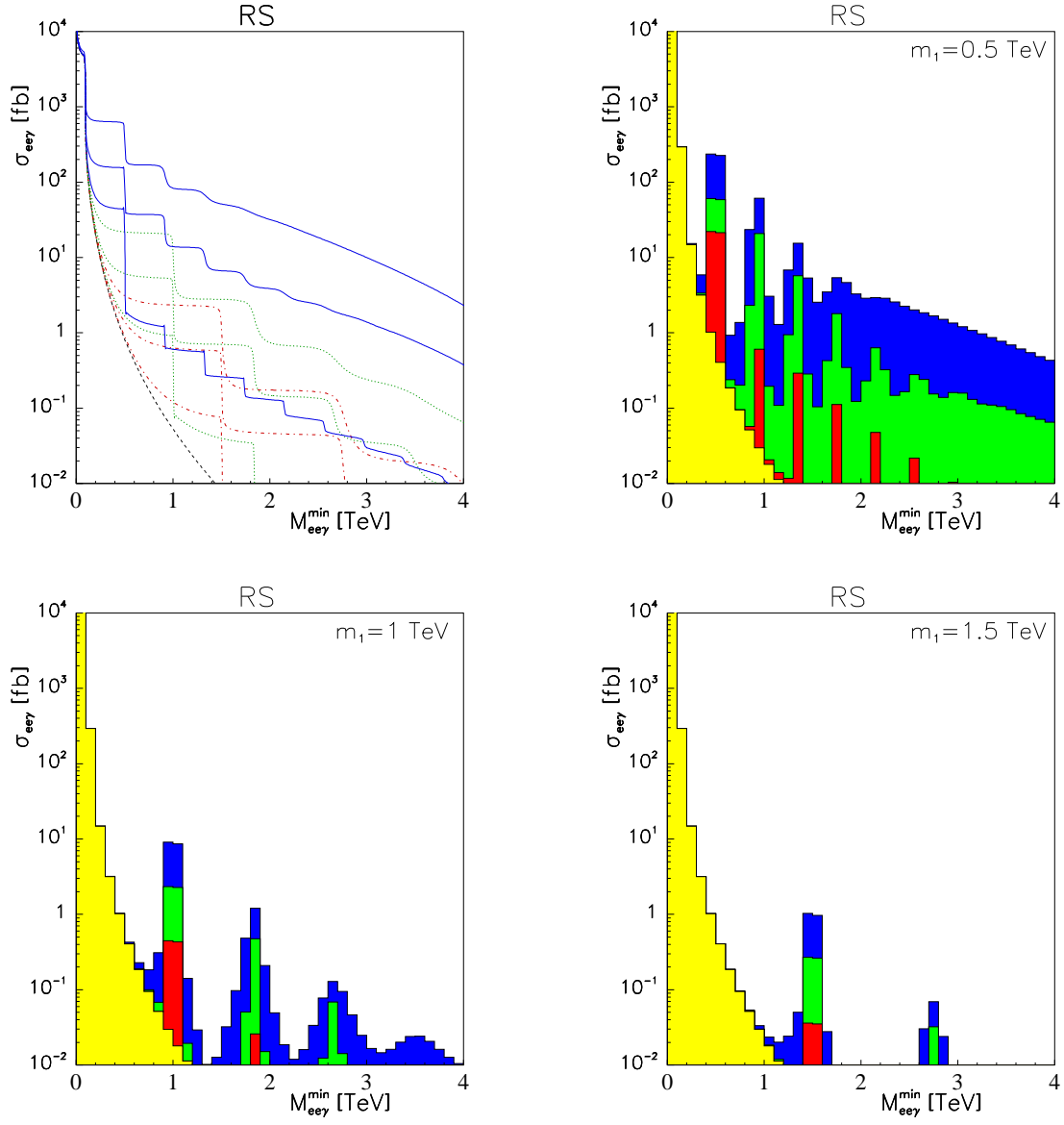


Figure 5: Integrated cross sections for the RS scenario. In the upper left panel we have integrated the cross sections in Fig. 4 over $\sqrt{\hat{s}}$ for $\sqrt{\hat{s}} \geq M_{ee\gamma}^{\min}$. The choice of parameters is $k/\overline{M}_{\text{Pl}} = 0.1, 0.05$ and 0.01 (from above) for $m_1 = 0.5$ (solid), 1 (dotted) and 1.5 TeV (dash-dotted). The SM background (dashed) is also shown. The other three panels show the corresponding result of integrating over 100 GeV bins, with $m_1 = 0.5$ (upper right), $m_1 = 1$ (lower left) and $m_1 = 1.5$ TeV (lower right).

Appendix A: Convolution Integrals and Event Shapes

In this Appendix, we define the convolution integrals and the event shapes used in our expressions. First, the convolution integrals are:

$$\begin{aligned}
I_{gg}(\hat{s}) &= \int_{-Y}^Y dy f_g \left(\sqrt{\frac{\hat{s}}{s}} e^y \right) f_g \left(\sqrt{\frac{\hat{s}}{s}} e^{-y} \right), \\
I_{q\bar{q}}(\hat{s}) &= 2 \sum_q \int_{-Y}^Y dy f_q \left(\sqrt{\frac{\hat{s}}{s}} e^y \right) f_{\bar{q}} \left(\sqrt{\frac{\hat{s}}{s}} e^{-y} \right), \\
I_{q\bar{q}}^{(\gamma)}(\hat{s}) &= 2 \sum_q Q_q^2 \int_{-Y}^Y dy f_q \left(\sqrt{\frac{\hat{s}}{s}} e^y \right) f_{\bar{q}} \left(\sqrt{\frac{\hat{s}}{s}} e^{-y} \right), \\
I_{q\bar{q}}^{(Z)}(\hat{s}) &= 2 \sum_q (v_q^2 + a_q^2) \int_{-Y}^Y dy f_q \left(\sqrt{\frac{\hat{s}}{s}} e^y \right) f_{\bar{q}} \left(\sqrt{\frac{\hat{s}}{s}} e^{-y} \right), \\
I_{q\bar{q}}^{(\gamma,Z)}(\hat{s}) &= 2 \sum_q Q_q v_q \int_{-Y}^Y dy f_q \left(\sqrt{\frac{\hat{s}}{s}} e^y \right) f_{\bar{q}} \left(\sqrt{\frac{\hat{s}}{s}} e^{-y} \right), \tag{A.1}
\end{aligned}$$

with

$$Y = \frac{1}{2} \log \frac{s}{\hat{s}}. \tag{A.2}$$

For the contribution from diagram 5, and also its interference with the photon, the convolution integral $I_{q\bar{q}}^{(\gamma)}(\hat{s})$ must be used, whereas for the interference of diagram 5 with Z , the relevant convolution integral is $I_{q\bar{q}}^{(\gamma,Z)}(\hat{s})$. Note the factor of two in the $q\bar{q}$ convolutions, which accounts for the fact that at a pp collider, either beam can provide the quark or the antiquark. All convolution integrals have been evaluated with CTEQ5 parton distribution functions [24].

The event shape distributions of the different contributions involve the following expressions:

$$\begin{aligned}
X_{\text{SM}}(x_1, x_2) &= 2(x_1^2 + x_2^2), \\
X_4(x_1, x_2) &= 2(x_1^2 + x_2^2)[16x_1x_2 - 6(x_1 + x_2) + 3], \\
X_5(x_1, x_2) &= x_3^2(1 - 2x_3)(3 - 4x_3) - (x_1 - x_2)^2(1 - 6x_3) - 8(x_1 - x_2)^4, \\
X_{5,\gamma}(x_1, x_2) &= X_{5,Z}(x_1, x_2) = 4(x_1^2 + x_2^2) - (x_1 + x_2), \tag{A.3}
\end{aligned}$$

with $x_3 = 1 - x_1 - x_2$.

Appendix B: Definition of y-cuts

Here we shall define quantities where the x_1, x_2 dependence (which determines event shapes) in the cross sections is integrated out. When we carry out these integrations,

we will impose y -cuts. In the case of gluon-gluon fusion, we define

$$S_{gg \rightarrow ee\gamma}^{(G)} = \iint_{s_i > y\hat{s}} dx_1 dx_2 \frac{X_4(x_1, x_2)}{(1-2x_1)(1-2x_2)(1-2x_3)}. \quad (\text{B.1})$$

These y -cuts will remove IR soft and collinear events where the photon has little energy, or its direction is close to that of an electron. The cut y_3 , which could be milder, will remove events where the two electrons are close.

In the case of quark-antiquark annihilation, the approach is the same, so we will not write out the integrals here. However, in the case of diagram 5 and the interference terms, $s_3 = (1-2x_3)\hat{s}$ depends on x_1 and x_2 (through x_3), so the graviton propagator as well as other factors involving s_3 must be part of the integrand.

References

- [1] I. Antoniadis, Phys. Lett. B **246** (1990) 377.
- [2] V. A. Rubakov and M. E. Shaposhnikov, Phys. Lett. B **125** (1983) 136;
 E. Witten, Nucl. Phys. B **443** (1995) 85 [hep-th/9503124];
 P. Hořava and E. Witten, Nucl. Phys. B **460** (1996) 506 [hep-th/9510209];
 P. Hořava and E. Witten, Nucl. Phys. B **475** (1996) 94 [hep-th/9603142].
- [3] N. Arkani-Hamed, S. Dimopoulos and G. Dvali, Phys. Lett. B **429** (1998) 263 [hep-ph/9803315];
 N. Arkani-Hamed, S. Dimopoulos and G. Dvali, Phys. Rev. D **59** (1999) 086004 [hep-ph/9807344].
- [4] L. Randall and R. Sundrum, Phys. Rev. Lett. **83** (1999) 3370 [hep-ph/9905221];
 L. Randall and R. Sundrum, Phys. Rev. Lett. **83** (1999) 4690 [hep-th/9906064].
- [5] G. F. Giudice, R. Rattazzi and J. D. Wells, Nucl. Phys. B **544** (1999) 3 [hep-ph/9811291].
- [6] E. A. Mirabelli, M. Perelstein and M. E. Peskin, Phys. Rev. Lett. **82** (1999) 2236 [hep-ph/9811337];
 S. Cullen, M. Perelstein and M. E. Peskin, Phys. Rev. D **62** (2000) 055012 [hep-ph/0001166].
- [7] T. Han, J. D. Lykken and R. Zhang, Phys. Rev. D **59** (1999) 105006 [hep-ph/9811350].
- [8] J. L. Hewett, Phys. Rev. Lett. **82** (1999) 4765 [hep-ph/9811356].
- [9] K. Cheung, Phys. Rev. D **61** (2000) 015005 [hep-ph/9904266].
- [10] H. Davoudiasl, J. L. Hewett and T. G. Rizzo, Phys. Rev. Lett. **84** (2000) 2080 [hep-ph/9909255].

- [11] H. Davoudiasl, J. L. Hewett and T. G. Rizzo, Phys. Rev. D **63** (2001) 075004 [hep-ph/0006041].
- [12] J. Bijnens, P. Eerola, M. Maul, A. Månsson and T. Sjöstrand, Phys. Lett. B **503** (2001) 341 [hep-ph/0101316].
- [13] J. Hewett and M. Spiropulu, [hep-ph/0205106].
- [14] G. Landsberg, [hep-ex/0105039].
- [15] D. Acosta *et al.* [CDF Collaboration], [hep-ex/0205057].
- [16] S. Hannestad and G. Raffelt, Phys. Rev. Lett. **87**, 051301 (2001) [hep-ph/0103201]; S. Hannestad and G. G. Raffelt, Phys. Rev. Lett. **88**, 071301 (2002) [hep-ph/0110067]; Y. Uehara, [hep-ph/0203244].
- [17] E. Dvergnes, P. Osland and N. Öztürk, in *Proc. XVIth International Workshop on High Energy Physics and Quantum Field Theory*, (QFTHEP'01, Moscow 2001), to be published [hep-ph/0108029].
- [18] E. Gabrielli and B. Mele, [hep-ph/0205099].
- [19] H. A. Olsen, P. Osland and I. Øverbø, Nucl. Phys. B **171** (1980) 209.
- [20] R. Contino, L. Pilo, R. Rattazzi and A. Strumia, JHEP **0106**, 005 (2001) [hep-ph/0103104].
- [21] See e.g., *ATLAS detector and Physical Performance Technical Design Report*, <http://atlasinfo.cern.ch/Atlas/GROUPS/PHYSICS/TDR/access.html>, G. L. Bayatian *et al.*, *CMS Technical Proposal*, CERN LHCC 94-38 (1994), <http://cmsinfo.cern.ch/TP/TP.html>.
- [22] B. C. Allanach, K. Odagiri, M. A. Parker and B. R. Webber, JHEP **0009**, 019 (2000) [hep-ph/0006114].
- [23] H. Davoudiasl and T. G. Rizzo, Phys. Lett. B **512**, 100 (2001) [hep-ph/0104199].
- [24] H. L. Lai *et al.* [CTEQ Collaboration], Eur. Phys. J. C **12**, 375 (2000) [hep-ph/9903282].